Journal of Physics:
Conference Series

PAPER • **OPEN ACCESS**

Geometric Modifications for Noise Mitigation in Axially Rotating Fan Blades

To cite this article: Saad-Eldin Taha *et al* 2025 *J. Phys.: Conf. Ser.* **3070** 012002

Geometric Modifications for Noise Mitigation in Axially Rotating Fan Blades

Saad-Eldin Taha[1*], Mohamed Y.Zakaria[2] and Mohamed Mahgoub Bassuoni[3]

[1] Mechanical Power Engineering Department, Faculty of Engineering Tanta University, Tanta, Egypt
[2] Military Technical College, Aerospace Department, Cairo, Egypt
[3]Mechanical Power Engineering Department, Faculty of Engineering Tanta University, Tanta, Egypt

[*]E-mail: saadeldeen147967@f-eng.tanta.edu.eg

Abstract. This study explores the effect of laminar and turbulent boundary layers, as well as boundary layer separation, on noise generation from an axial rotating blade of a ducted fan. Quieter fans provide significant advantages in terms of regulatory compliance, comfort, efficiency, safety, health, and sustainability across industries like aviation and HVAC. Additionally, reducing noise pollution and its impact on the ecosystem, along with minimizing vibrations and wear, can extend the lifespan of components. This investigation was conducted using a case study of a seven-blade axial fan designed by CF Turbo software. The study examines the impact of reducing the chord length from 7.5 cm at the root to 3.56 cm at the tip on noise generation at a constant rpm. A comparative analysis was also carried out between the sound generated by the original and modified blades, revealing a noticeable 28% reduction in the peak overall sound power level.

1. Introduction

Aeroacoustics constitutes the discipline devoted to the examination of sound emanating from the interaction between airflow and solid surfaces. This sound can manifest as either a discrete pure tone or a broad spectrum of frequencies, necessitating a thorough investigation into its origins. The selection of observation points also bears significance consideration. An understanding of the overall sound power level is imperative, achievable through either computational modelling or empirical testing. Subsequently, measures to regulate or mitigate noise emission become imperative, given the potential for heightened irritation among individuals subjected to excessive noise levels, particularly in contexts involving direct exposure to sources such as HVAC system fans, wind turbines, and aircraft propellers.

Over time, scientists involved in this field have yielded diverse methodologies for the assessment and prediction of noise generated by blade systems. These encompass numerical, analytical, and semi-analytical techniques, as well as semi-empirical and computational approaches, notably exemplified by computational aeroacoustics (CAA).

During the early stages of design it is very important to estimate the noise generated through easy and inexpensive way. Before the specific illustration of the airfoil noise the main sources of noise (categories) should be illustrated first. The sources of noise (monopole, dipole, quadrupole) are the main classifications of sound creating, thus describing each through mathematical equations would help in prediction of the intensity of sound created [1].

Aerodynamic noise would be either a pure tone or a broadband noise. The pure tone in case of fans, propellers and wind turbines for example will be the blade passing frequency. According to aerodynamic broadband noise that is generated are classified as follows:

- Turbulent boundary layer trailing edge (TBL-TE) noise
- Laminar boundary layer vortex shedding (LBL-VS) noise
- Tip vortex formation noise
- Trailing edge bluntness vortex shedding noise
- Separation-stall noise

These five sources are considered airfoil self-noise. In case of ducted fan tip vortex formation noise will be out of concern as the ducted fans are widely used nowadays because of their lower acoustic signature compared to other fans [2] also trailing edge bluntness vortex shedding noise will be neglected assuming sharp trailing edged blade.

In the nascent stages of this field, the calculation of sound generation was primarily established through the groundbreaking efforts of Sir Lighthill, who adeptly rearranged the Navier–Stokes equation. This method, along with Curle's and Ffowcs Williams–Hawkings analogies, is regarded as the analytical solution to aeroacoustics. These analytical solutions have been instrumental in computational approaches, particularly within computational aeroacoustics (CAA).

Subsequently, significant strides were made in experimental research by Thomas F. Brooks, D. Stuart Pope and Michael A. Marcolini (BPM) [3], which elucidated the five primary sources of airfoil self-noise. Through meticulous experimentation, alongside illustrative measurements, empirical formulas were devised for calculating the sound power level (SPL) of each source. This pioneering work underpinned the development of various software packages, such as NREL AirFoil Noise (NAFnoise) [4], aimed at predicting SPL for four of these five sources (TBL-TE, LBL-VS, trailing edge bluntness vortex shedding noise and separation stall noise) and the overall sound power level (OASPL) at specific observation points. These packages offer the flexibility to select boundary layer data either from XFOIL (developed by Drela [5]), or from the empirical findings of the Brooks, Pope, Marcolini (BPM) model. Trailing edge noise from turbulent boundary layers can be addressed through the Netherlands Organization for Applied Scientific Research model (TNO model) [6].

BPM model was chosen for the aeroacoustic solution in this study as it is concerned with the three sources of noise that we focus on during the aeroacoustic solution.

2. BPM model

2.1 TBL-TE noise and separated flow noise

TBL-TE Noise is generated as this turbulence passes over the trailing edge and it is considered one of the most important sources of noise generated that's why it is the point of interest. TBL-TE noise and separated flow noise, which in this model is decomposed into three primary components: pressure side, suction side, and angle of attack (separated flow), each represented by the following equations

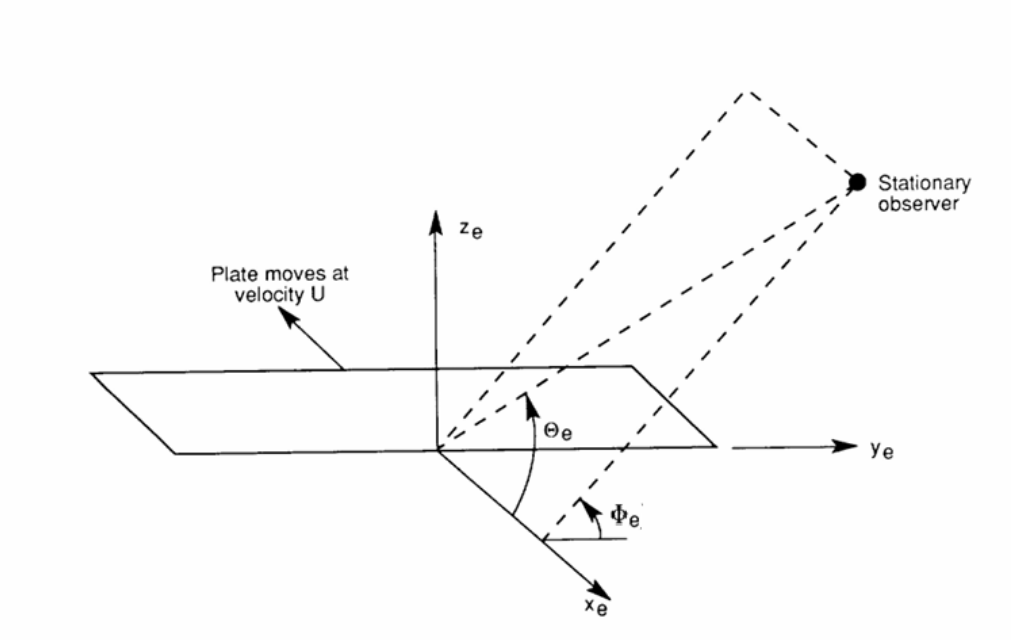

Figure 1. Angles used in the directivity function.

$$\mathrm{SPL_{TBL\text{-}TE}} = 10\log_{10}\left(10^{\frac{\mathrm{SPL_p}}{10}} + 10^{\frac{\mathrm{SPL_s}}{10}} + 10^{\frac{\mathrm{SPL_\alpha}}{10}}\right) \quad (1)$$

$$\mathrm{SPL_p} = 10\log_{10}\left(\frac{\delta_p^* M^5 d\overline{D_h}}{r_e^2}\right) + A\left(\frac{\mathrm{St_p}}{\mathrm{St_1}}\right) + (K_1 - 3) + \Delta K_1 \quad (2)$$

$$\mathrm{SPL_s} = 10\log_{10}\left(\frac{\delta_s^* M^5 d\overline{D_h}}{r_e^2}\right) + A\left(\frac{\mathrm{St_s}}{\mathrm{St_1}}\right) + (K_1 - 3) \quad (3)$$

$$(prestall)\mathrm{SPL_\alpha} = 10\log_{10}\left(\frac{\delta_s^* M^5 d\overline{D_h}}{r_e^2}\right) + B\left(\frac{\mathrm{St_s}}{\mathrm{St_2}}\right) + K_2 \quad (4)$$

$$(poststall)\mathrm{SPL_\alpha} = 10\log_{10}\left(\frac{\delta_s^* M^5 d\overline{D_l}}{r_e^2}\right) + A'\left(\frac{\mathrm{St_s}}{\mathrm{St_2}}\right) + K_2 \quad (5)$$

$$St_p = \frac{f\delta_p^*}{U}, St_\mathrm{s} = \frac{f\delta_s^*}{U} \quad (6)$$

where, (δ_p^* , δ_s^*) are the boundary layer displacement thickness on either side of the airfoil (pressure and suctions sides), (M)$ is the Mach number, (d) is the span wise extent wet by the flow, (r_e) is the observer distance measured value, (St) is the Strouhal number, as the Strouhal number (St_p) and (St_s) is based on (δ_p^*) and (δ_s^*), where (f) is frequency of the vortex shedding or oscillations (in Hz) and (U) is free-stream velocity of air, (St_1) if function in Mach number and (St_2) is function in (St_1) and (α^*) which is angle of attack after wind tunnel correction, (A, A', B) are spectral terms, ($\Delta K_1, K_1$") and (K_2) are scaling terms, both spectral and scaling terms were discussed in details in reference [3]. Also, the directivity term ($\overline{D}$) which is function in the observer's position angels as it corrects the SPL depending on the relative position of the observer to the emitter as shown in Figure 1 (h, l are for high frequency and low frequency respectively), all the above terms were discussed in details in reference [3]. where the directivity terms can be expressed as follows,

$$\overline{D_h}(\Theta_e, \Phi_e) = \frac{2\sin^2\left(\frac{\Theta_e}{2}\right)\sin^2\Phi_e}{(1 + M\cos\Theta_e)(1 + (M - M_c)\cos\Theta_e)^2} \quad (7)$$

$$\overline{D_l}(\Theta_e, \Phi_e) = \frac{\sin^2\Theta_e \sin^2\Phi_e}{(1 + M\cos\Theta_e)^4} \quad (8)$$

2.2 LBL-VS noise

LBL-VS it depends on the type of the flow on the pressure side and suction side of the airfoil when reaching the trailing edge (last point on the flow path when passing by an airfoil) that's why studying the flow behavior through all phases of airfoil passing path is important, as the transition point and inflection point (which will be important in the determination of separation stall noise), LBL-VS noise is represented in the following empirical equation.

$$\mathrm{SPL}_{\text{LBL-VS}} = 10\log_{10}\left(\frac{\delta_p M^5 d\overline{D_h}}{r_e^2}\right) + G_1\left(\frac{St'}{St'_{\text{peak}}}\right) + G_2\left[\frac{Re_c}{(Re_c)_0}\right] + G_3(\alpha_*) \quad (9)$$

where, (δ_p) is the BL thickness (pressure side), (G_1) defines the spectral shape in terms of the ratio of strouhal number to its peak, $St' = \frac{f\delta_p}{U}$ and $St'_{\text{peak}} = St_1{}' \times 10^{-0{,}04\alpha^*}$ where $\left(St'_{\text{peak}}\right)$ is the peak Strouhal number, Strouhal number (St'_1) is function in (Re_c) which is the Reynolds number at chord (c_i), (G_2) is the peak scaled level shape curve depends on Reynolds number and angle (α^*), (G_3) is the angle (α^*) dependent level for the shape curve, The subscript $(\mathbf{0})$ refers to a reference Reynolds number that is a function of (α^*), all of these functions are discussed in reference [3] where represents empirical functions.

3. Axial inducted fan case study

3.1 Blade design and aerodynamic characteristics

Figure 2. Axial fan.

A shrouded axial fan of seven blades Figure 2. The basic data of the blade is shown in Table 1, the

Table 1. Blade parameters.

Sec.	Radius (m)	Vrel (m/s)	Vrel angel (deg.)	M	AoA (deg.)	Chord (m)	Cl	Twist angle (deg.)	Re
Sec 1 Root	0.098	41	1.4	0.12	5	0.075	0.625	6.4	203,035
Sec 2	0.137	57.6	1	0.17	5	0.075	0.633	6	286,184
Sec 3 middle	0.177	74.3	0.8	0.22	5	0.075	0.660	5.8	369,342
Sec 4	0.217	91	0.6	0.27	5	0.075	0.642	5.6	452,503
Sec 5 Tip	0.257	107.8	0.5	0.32	5	0.075	0.651	5.5	535,666

blade is divided to 5 sections (4 segments) with design point at 4000 rpm and inlet flow speed of 1 m/s and hub tip ratio of 0.37.

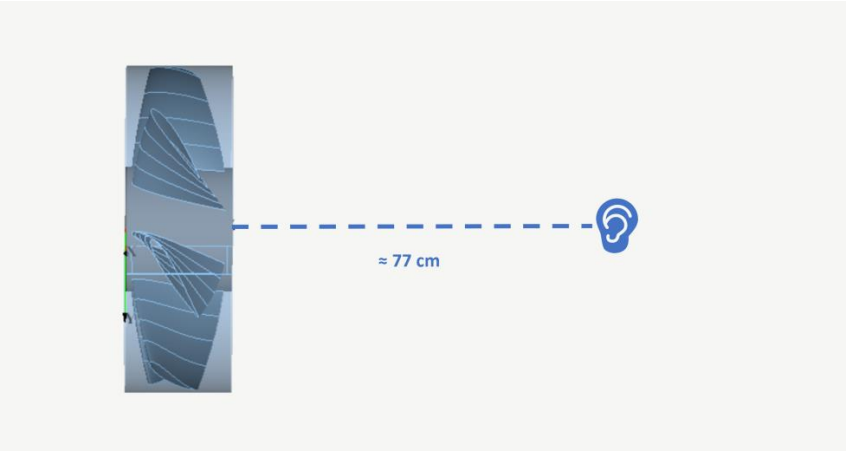

Figure 3. Point of observation.

3.2 Blade geometry modification

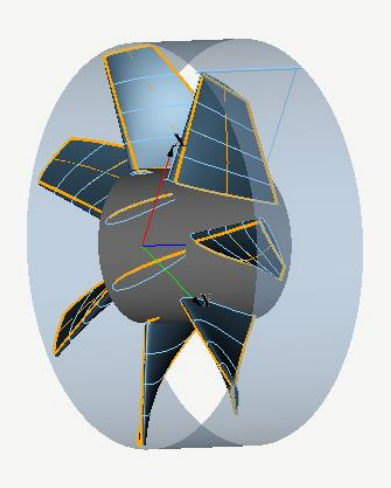

Figure 4. Modified Blades fan.

Regarding chord length per section, by modifying the blade by decreasing the chord length from 7.5 cm at the root to 3.56 cm at the tip as shown in Figure 4, the geometric data of the modified fan is shown in Table 2.

Table 2. Modified blade parameters.

Sec.	Radius (m)	Vrel (m/s)	Vrel angel (deg.)	M	AoA (deg.)	Chord (m)	Cl	Twist angle (deg.)	Re
Sec 1 Root	0.098	41	1.4	0.12	5	0.075	0.625	6.4	203,035
Sec 2	0.137	57.6	1	0.17	5	0.065	0.633	6	248,458
Sec 3 middle	0.177	74.3	0.8	0.22	5	0.055	0.660	5.8	272,457
Sec 4	0.217	91	0.6	0.27	5	0.045	0.642	5.6	274,153
Sec 5 Tip	0.257	107.8	0.5	0.32	5	0.0356	0.651	5.5	254,209

3.3 Aeroacoustic solution setup

The influence of changing the chord length on sources of noise and the influence of these changes on blades OASPL also will be discussed. Choosing BPM model for calculating the 1/3 octave SPL for rotating blade through dividing the blade into four segments as shown in Figure 2 each segment will be solved separately then combining the results together to get the SPL at an observing point then comparing the results before and after changing the blades geometry. Choosing the point of observation is very important as it must be in the far-field and taking into consideration the Doppler effect in case of rotating blades. NREL AirFoil Noise (NAFnoise) [3] used to solve BPM model, boundary layer data will be calculated using XFOIL, also the point of observation is 77 cm on the axis of rotation in order to minimize the Doppler effect as shown in Figure 3.

3.4 Boundary layer features

Boundary layer depends on the type of the flow on the pressure side and suction side of the airfoil when reaching the trailing edge (last point on the flow path when passing by an airfoil) that's why studying the flow behaviour through all phases of airfoil passing path is important, as the transition point and inflection point (which will be important in the determination of separation stall noise). Through observing the displacement thickness of boundary layer (δ^*) through which the abrupt decrease in (δ^*) indicates the transition point from laminar boundary layer to turbulent one (these points are marked with dashed circles) for original blade suction side where boundary layer for all sections turned to be turbulent as shown in Figure 5, but for pressure side

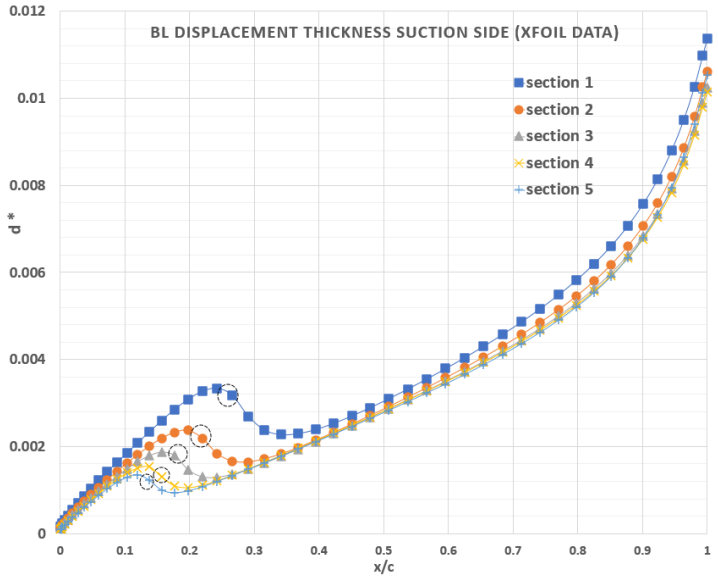

Figure 5. δ_s^* Vs x/c for suction side.

boundary layer is laminar for all sections till the trailing edge as shown in Figure 6.

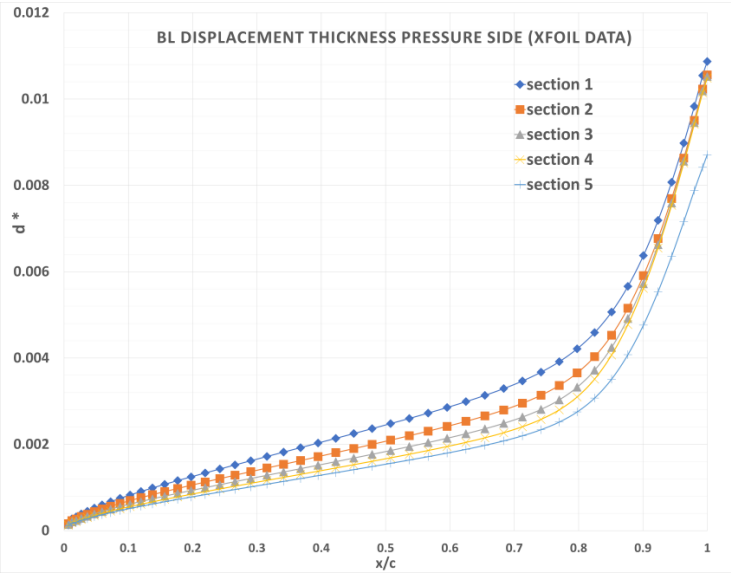

Figure 6. δ_p^* Vs x/c for pressure side.

For modified blade also boundary layer for suction side of all sections turned to be turbulent as shown in Figure 7, for pressure side boundary layer is laminar for all sections till the trailing edge Figure 8.

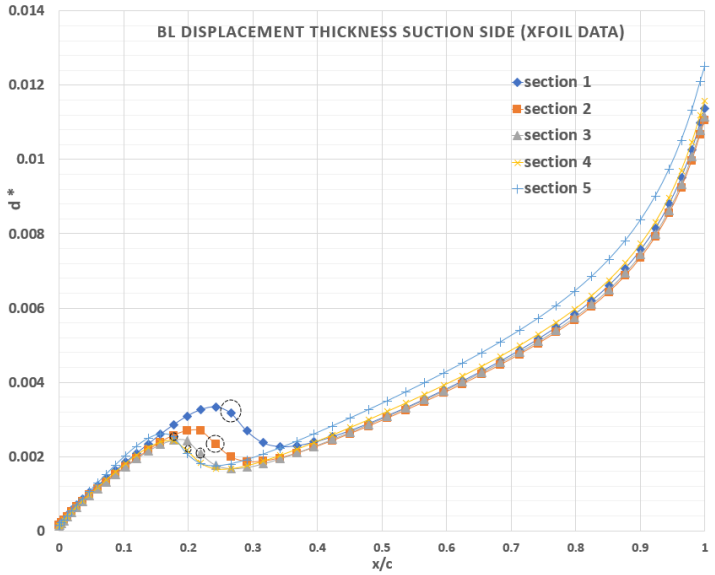

Figure 7. δ_s^* Vs x/c for suction side.

3.5 Separated flow sections

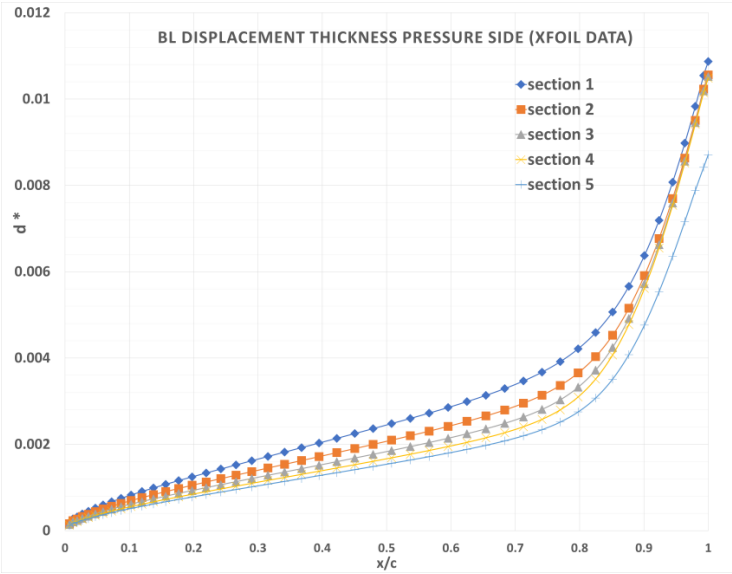

Figure 8. δ_p^* Vs x/c for pressure side.

Upon observing the skin friction coefficient of suction side and pressure side of the original blade Figure 9 and Figure 10, a detailed examination of the XFOIL data reveals that the flow has separated in this region characterized by $C_f < 0$, resulting in a slow recirculation within a separation bubble (recirculating region) [7]. Through sections 1 to 5 flow is separates and re-attaches again for suction side and for pressure side the flow seems to separate for all sections near 0.9% of the chord and then re-attaches at tailing edge.

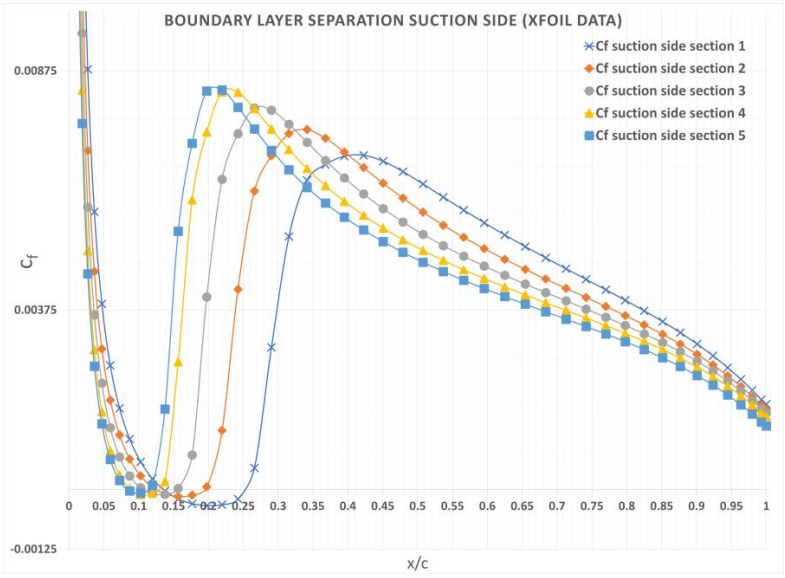

Figure 9. C_f Vs x/c for suction side.

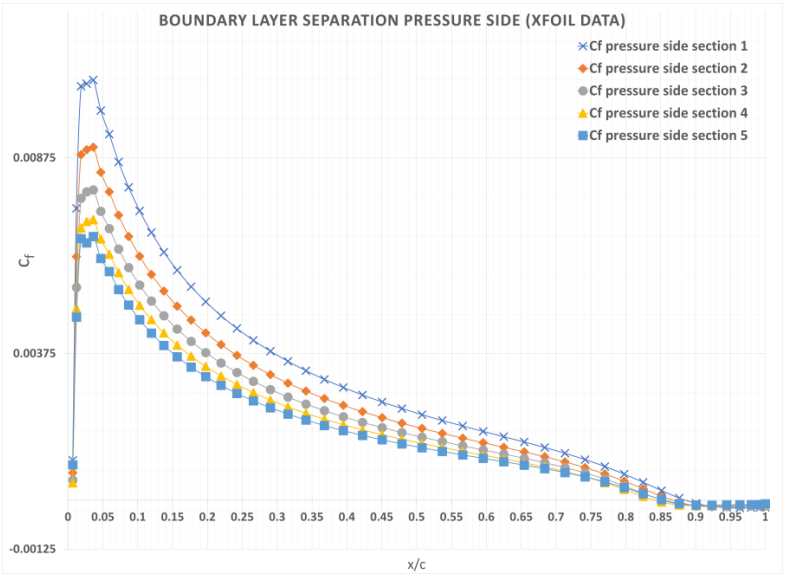

Figure 10. C_f Vs x/c for pressure side.

For the modified blade as shown in Figure 11 and Figure 12 also separation happens for suction side through all sections and reattaches again and for the pressure side the flow also seems to separate for all sections near 0.9% of the chord and then re-attaches at tailing edge.

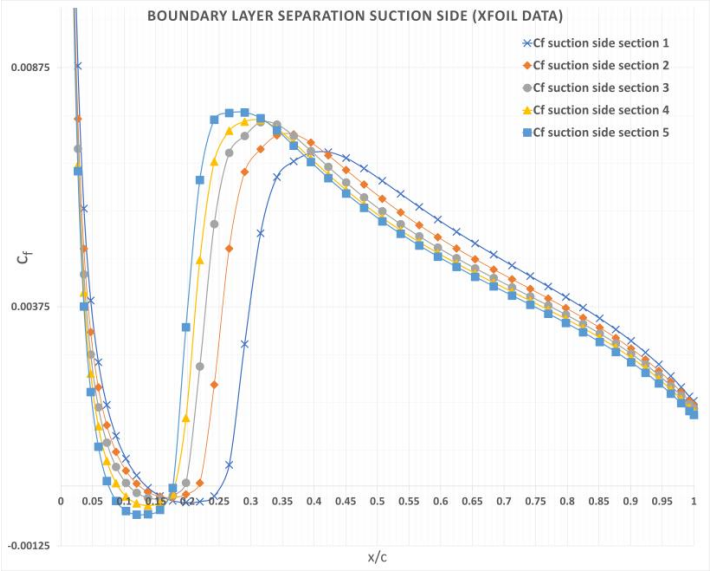

Figure 11. C_f Vs x/c for suction side.

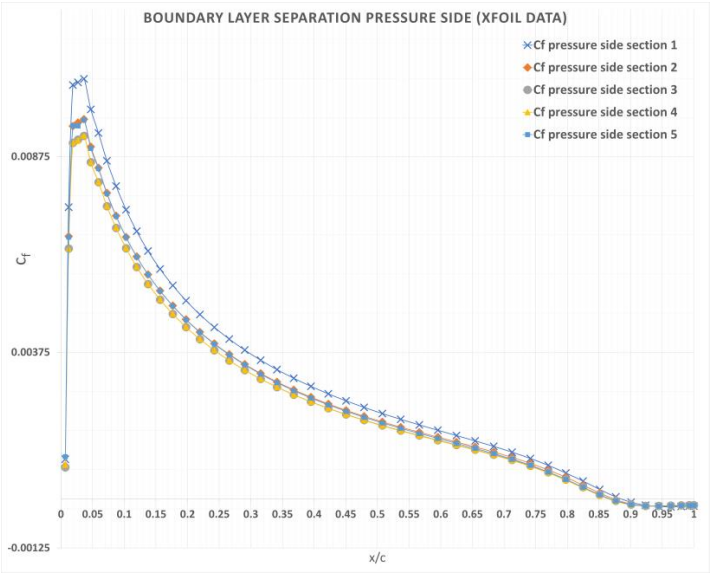

Figure 12. C_f Vs x/c for pressure side.

3.6 Aeroacoustic solution

According to the previous aerodynamic analysis it is shown that the only sources of noise that are in concern are TBL-TE (for suction side), LBL-VS (for pressure side) and separation noise (for suction side). The comparison between the noise generated from segments before and after modification is shown through tables from Table 3 to Table 6 and figures from Figure 13 to Figure 20.

3.6.1 Segment 1

Table 3 shows the comparison between the noise generated from segments before and after modification and the 1/3 octave SPL of these sources is shown in Figure 13 for original blade and Figure 14 for modified blade.

Table 3. Segment 1 original and modified blades Modified blades comparison.

	Original blade	Modified blade
TBL-TE suction side	Peak (4000 Hz , 41.541 dB)	Peak (4000 Hz , 44.928 dB)
LBL-VS pressure side	Peak (5000 Hz , 38.368 dB)	Peak (6300 Hz , 46.244 dB)
Separation suction side	Peak (4000 Hz , 44.717 dB)	Peak (5000 Hz , 48.505 dB)
OASPL	Peak (4000 Hz , 47.012 dB)	Peak (4000 Hz , 50.646 dB)

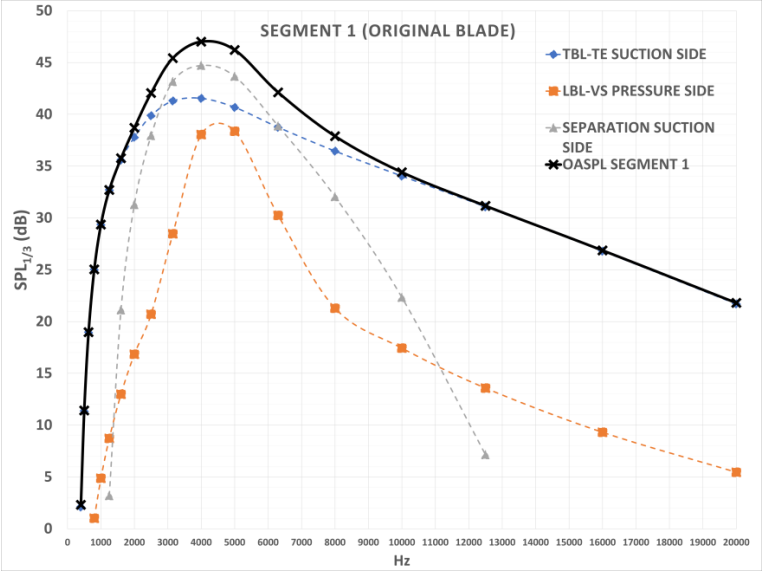

Figure 13. Segment 1 original blade.

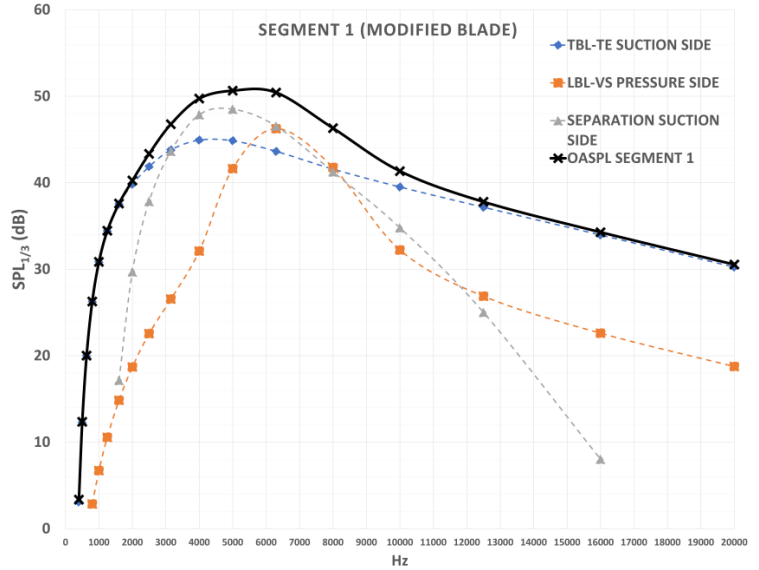

Figure 14. Segment 1 modified blade.

3.6.2 Segment 2

Table 4 shows the comparison between the noise generated from segments before and after modification and the 1/3 octave SPL of these sources is shown in Figure 15 for original blade and Figure 16 for modified blade.

Table 4. Segment 2 original and modified blades Modified blades comparison.

	Original blade	Modified blade
TBL-TE suction side	Peak (5000 Hz , 49.971 dB)	Peak (6300 Hz , 50.066 dB)
LBL-VS pressure side	Peak (10000 Hz , 62.686 dB)	Peak (10000 Hz , 55.546 dB)
Separation suction side	Peak (5000 Hz , 54.085 dB)	Peak (6300 Hz , 54.346 dB)
OASPL	Peak (10000 Hz , 62.686 dB)	Peak (10000 Hz , 55.546 dB)

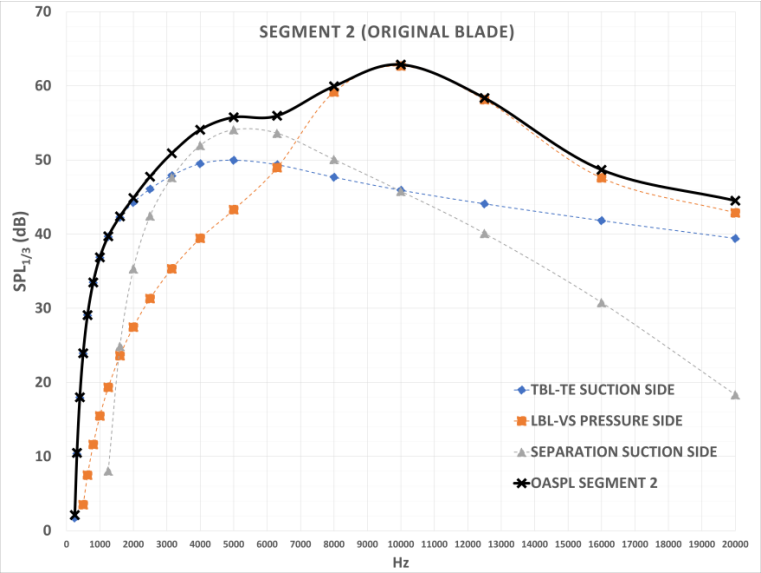

Figure 15. Segment 2 original blade.

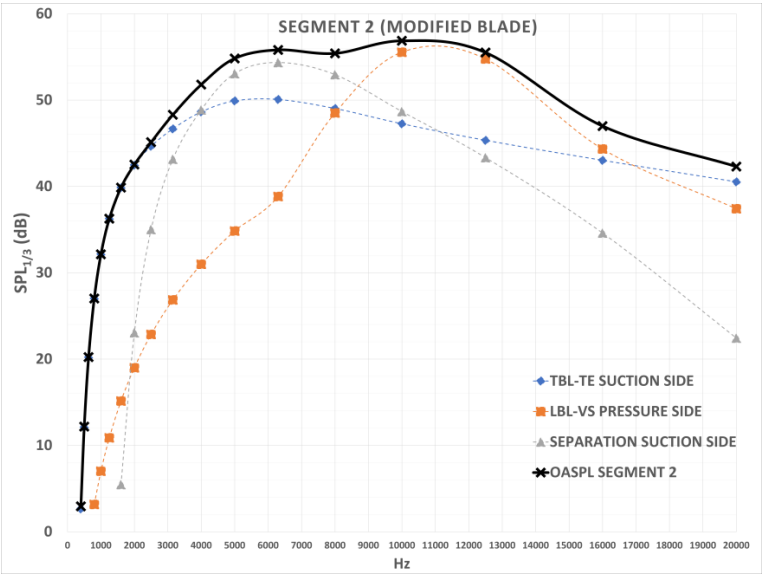

Figure 16. Segment 2 modified blade.

3.6.3 Segment 3

Table 5 shows the comparison between the noise generated from segments before and after modification and the 1/3 octave SPL of these sources is shown in Figure 17 for original blade and Figure 18 for modified blade.

Table 5. Segment 3 original and modified blades Modified blades comparison.

	Original blade	Modified blade
TBL-TE suction side	Peak (5000 Hz , 53.628 dB)	Peak (8000 Hz , 53.971 dB)
LBL-VS pressure side	Peak (12000 Hz , 73.295 dB)	Peak (16000 Hz , 60.981 dB)
Separation suction side	Peak (6000 Hz , 58.476 dB)	Peak (8000 Hz , 58.817 dB)
OASPL	Peak (12000 Hz , 73.326 dB)	Peak (16000 Hz , 61.463 dB)

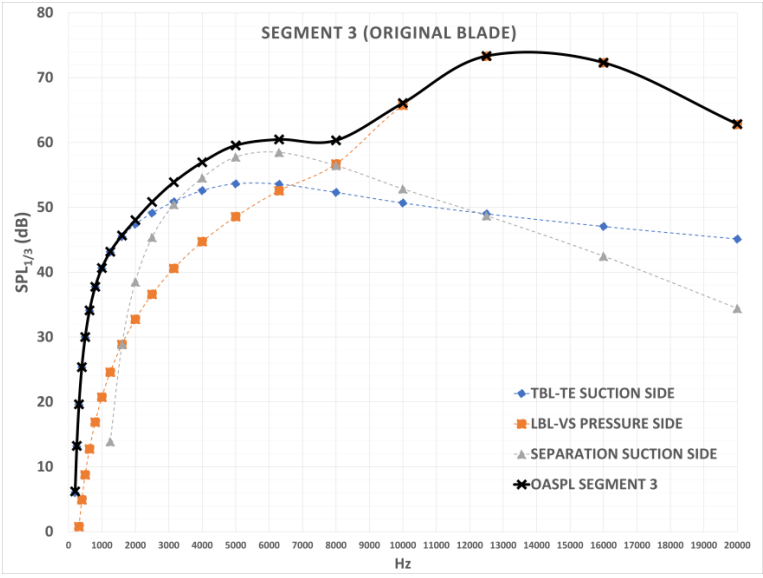

Figure 17. Segment 3 original blade.

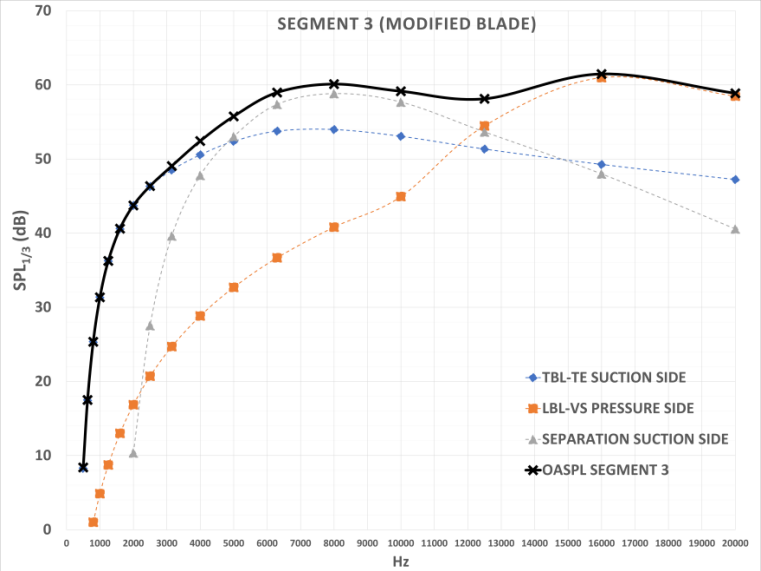

Figure 18. Segment 3 modified blade.

3.6.4 Segment 4

Table 6 shows the comparison between the noise generated from segments before and after modification and the 1/3 octave SPL of these sources is shown in Figure 19 for original blade and Figure 20 for modified blade.

Table 6. Segment 3 original and modified blades Modified blades comparison.

	Original blade	Modified blade
TBL-TE suction side	Peak (6300 Hz , 56.871 dB)	Peak (10000 Hz , 57.240 dB)
LBL-VS pressure side	Peak (16000 Hz , 80.173 dB)	Peak (20000 Hz , 60.394 dB)
Separation suction side	Peak (6300 Hz , 62.21 dB)	Peak (10000 Hz , 62.559 dB)
OASPL	Peak (16000 Hz , 80.181 dB)	Peak (10000 Hz , 63.697 dB)

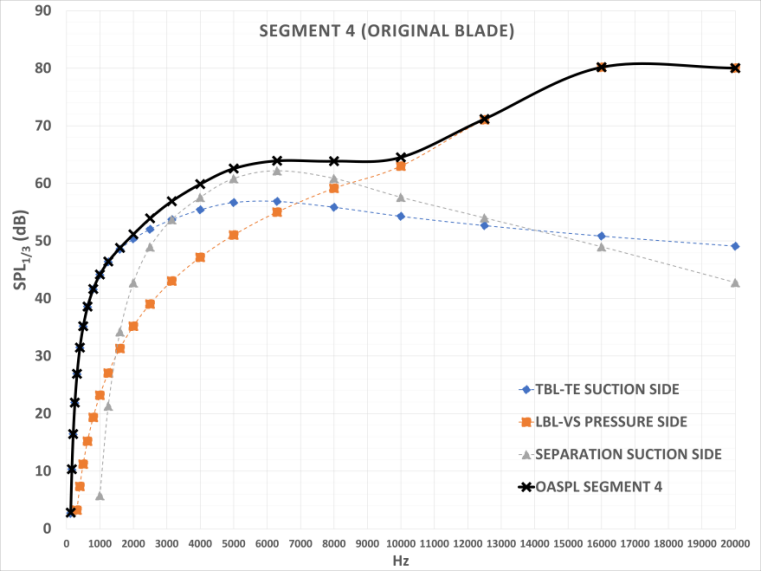

Figure 19. Segment 4 original blade.

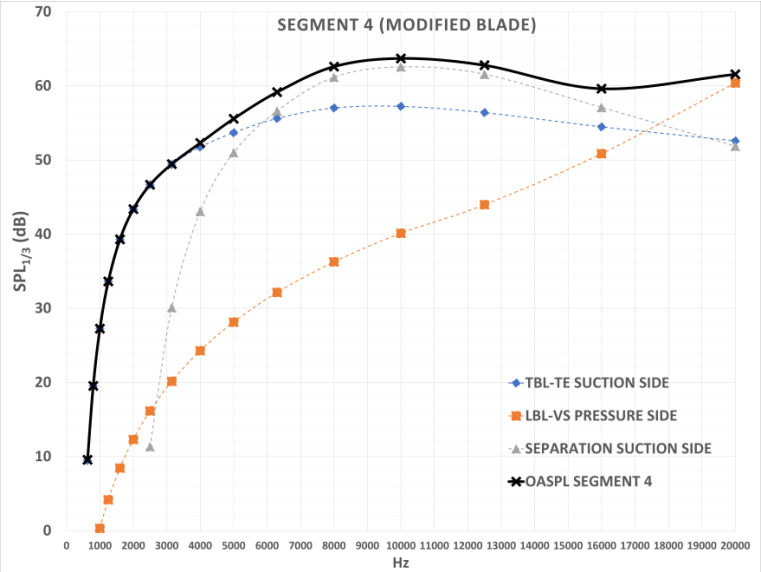

Figure 20. Segment 4 modified blade.

3.7 OASPL of the seven blades fan

The changes done to the geometry of the blades with respect to the chord lengths of the blades cross sections, it is clear that the OASPL across the whole frequency spectrum of the modified blades fan was much lower than the original blades fan as shown in Figure 21. As the original fan peak 1/3 octave SPL was 89.3 dB at 16 KHz, where the modified fan was 63.7 dB at 10 KHz.

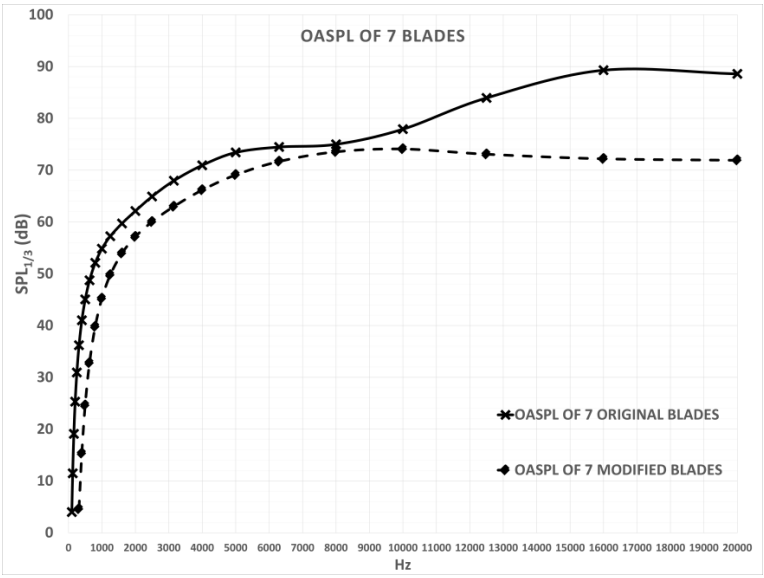

Figure 21. OASPL of the seven blades fan.

4. Conclusion

In conclusion, the low aeroacoustics modified fan demonstrates significant improvements in noise reduction when compared to the original fan design. By optimizing key aerodynamic features such as blade shape, the modified fan successfully minimizes the OASPL of the fan and this leads to a quieter operation, making the modified fan ideal for applications where noise reduction is necessary, such as in HVAC systems and aviation. Additionally, the modification does not sacrifice performance, as the fan continues to maintain or even enhance its efficiency, demonstrating that aeroacoustic optimization can be achieved without compromising functionality. Thus, the low aeroacoustics modified fan offers a balanced solution that prioritizes both noise control and performance, representing a step forward in fan technology.

References

[1] Jack E. Marte, D. W. (January 1, 1970). A Review of Aerodynamic Noise From Propellers, Rotors, and Lift Fans (Technical Report 32-1462). Pasadena, California: Jet Propulsion Laboratory, California Institute of Technology.
[2] Nemnem, A. F., Zakaria, M. Y., Elzahaby, A. M. 2018, 'Contra-rotating Ducted Fan Aerothermodynamic Design Procedure for Unmanned Applications', AIAA Information Systems-AIAA Infotech @ Aerospace Conference, Kissimmee, FL, January 8–12, 2018, AIAA-2018-0745.
[3] Thomas F. Brooks, D. Stuart Pope and Michael A. Marcolini, {Airfoil Self-Noise and prediction.}, NASA reference publications 1218, (July 1989).
[4] Patrick Moriarty, National Wind Technology Center National Renewable Energy Laboratory Golden, Colorado, (July 2005).
[5] Drela M. and Giles M., "Viscous-Inviscid Analysis of Transonic and Low Reynolds Number Airfoils," AIAA Journal, Vol. 25, No. 10, 1987.
[6] Moriarty, P. and Migliore, P., Semi-Empirical Aeroacoustic Noise Prediction Code for Wind Turbines, NREL/TP-500-34478, National Renewable Energy Laboratory, Golden, CO, 2003.
[7] Iliev, S. P. (2016). Aerofoil analysis using XFOIL - Practical implementation for preliminary wing design. Imperial College London.